J. Opt. **12** (2010) 124006 (8pp) doi:10.1088/2040-8978/12/12/124006

Optomechanics of liquid crystals for dynamical optical response of photonic structures

A E Miroshnichenko[1], E Brasselet[2], D O Krimer[3] and Yu S Kivshar[1]

[1] Nonlinear Physics Centre and Centre for Ultra-high bandwidth Devices for Optical Systems (CUDOS), Australian National University, Canberra ACT 0200, Australia
[2] Centre de Physique Optique Moléculaire et Hertzienne, Université Bordeaux 1, CNRS, 351 Cours de la Libération, 33405 Talence Cedex, France
[3] Max Planck Institute for the Physics of Complex Systems, Nöthnitzer Straße 38, D-01187 Dresden, Germany

E-mail: e.brasselet@cpmoh.u-bordeaux1.fr

Received 16 February 2010, accepted for publication 1 July 2010
Published 11 November 2010
Online at stacks.iop.org/JOpt/12/124006

Abstract
We show that the mechanical effect of light on the orientational ordering of the crystalline axis of a mesophase can be used to control the dynamics of the optical response of liquid crystal infiltrated photonic structures. The demonstration is made using a one-dimensional periodic structure whose periodicity is broken by the presence of a nematic liquid crystal defect layer. In this study we report on output light polarization and/or intensity dynamics that depend on the initial molecular ordering and incident light wavelength and intensity.

Keywords: liquid crystal infiltrated photonic structures, tunable photonic crystals, dynamical optical response, nonlinear optics of liquid crystals

(Some figures in this article are in colour only in the electronic version)

1. Introduction

Two decades ago, Yablonovitch [1] and John [2] independently introduced the concept of photonic crystals, i.e. dielectric systems with spatial periodicity of the refractive index, which led to the formation of photonic bandgaps. The latter correspond to wavevector ranges (hence implying direction and frequency), for which light cannot propagate. Indeed, this feature allows us to control the flow of light [3] provided there are appropriate structured material properties. To do so, the light itself offers practical solutions towards high-resolution three-dimensional optical micro- and nano-fabrication techniques [4]. Although being a necessary first step, structured material is, however, not enough when flexible optical data processing is envisaged, which requires reconfigurable photonic crystals. To do so, linear or nonlinear refractive index changes have appeared as a straightforward solution that can be supplied by external fields of different nature (e.g. thermal, electrical, or optical). Obviously, the use of light itself is appealing since it naturally benefits from the strong spatial confinement of the field inside the structure, thereby enhancing the optical response and paving the way towards all-optical photonic circuitry [5].

Among various nonlinear optical materials, the attractiveness of liquid crystals results from the genuine combination of its 'liquid' and 'crystalline' features, which allow easy integration into photonic crystal micro-architectures and extreme sensitivity to external fields at the same time. Such a possibility has been thoroughly studied since the pioneering results of, on the one hand, Busch and John, who proposed to use the orientational ordering of the optical axis of liquid crystals in order to tune the properties of photonic bandgaps [6], and, on the other hand, Yoshino *et al*, who proposed to benefit from the successive appearance of distinct mesophases in thermotropic liquid crystals when temperature is changed [7]. However, neither thermal nor electrical tuning of liquid crystals benefits from the very nature of a photonic crystal, contrary to the use of light itself to trigger refractive index changes.

The large orientational optical nonlinearities of liquid crystals [8, 9] can be fruitfully exploited to control the optical response of a photonic structure via the light that propagates inside it. Such an issue was addressed in previous works in the simplest case of a one-dimensional dielectric structure in which is embedded a pure or dye-doped nematic liquid crystal layer with initial uniform alignment [10–13]. These works, however, have only reported on static or transient light-induced changes. More recently, rotational dynamics of the director (i.e. the unit vector **n** that represents the local average molecular orientation of a nematic) has also been experimentally demonstrated [14].

In this study, we theoretically demonstrate that optomechanical effects at the mesoscale can be used to control output light polarization and/or intensity dynamics of liquid crystal infiltrated photonic structures. First we introduce the system in section 2.1 and the choice of two representative light–matter interaction geometries is discussed in section 2.2. Then, the optical threshold behavior is addressed in section 3. The all-optical dynamical response of the photonic structures is studied in section 4 and section 5 concludes the paper.

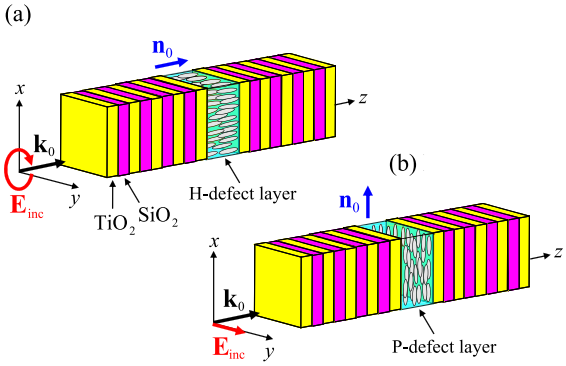

Figure 1. Definition of the homeotropic (a) and planar (b) geometries. They consist of a one-dimensional multilayered structure made of SiO_2 and TiO_2 in which is embedded a nematic liquid crystal layer. The uniform spatial distribution of its optical axis at rest is $\mathbf{n}_0 = \mathbf{e}_z$ in the case H and $\mathbf{n}_0 = \mathbf{e}_x$ in the case P. The excitation light beam impinges at normal incidence onto the structures, $\mathbf{k}_0 = k_0\mathbf{e}_z$, and the incident polarization state is set to circular in the case H, $E_{inc} = E_0(\mathbf{e}_x + i\mathbf{e}_y)/\sqrt{2}$, and to linear in the case P, $\mathbf{E}_{inc} = E_0\mathbf{e}_y$.

2. Background

2.1. Definitions

We choose a one-dimensional periodic structure made of alternating layers of SiO_2 and TiO_2 with thicknesses 103 and 64 nm, respectively, which exhibits a bandgap in the visible range between 500 and 720 nm. In all our simulations, a uniformly aligned nematic liquid crystal defect layer with thickness $L = 5\ \mu$m is located in the central part of the structure with five SiO_2/TiO_2 building blocks on each side (see figure 1). Our choice for the defect layer thickness corresponds to the obtainment of a few defect modes in the bandgap region that are characterized by a free spectral range much larger than the individual spectral linewidth (see later figure 4). Moreover, note that the present theoretical framework for the optical reorientation of liquid crystals neglects surface effects at the film input/output facets. This prevents an accurate description when the liquid crystal thickness is reduced to sub-micron scale. Qualitative expectations, however, could be inferred from the present study.

We consider two different kinds of initial uniform alignment $\mathbf{n}_0$ for the director. Namely, the initial alignment is either perpendicular (homeotropic anchoring, 'H') or parallel (planar anchoring, 'P') to the nematic slab. Hence, $\mathbf{n}_0 = \mathbf{e}_z$ or $\mathbf{n}_0 = \mathbf{e}_x$, where $(\mathbf{e}_x, \mathbf{e}_y, \mathbf{e}_z)$ is the Cartesian coordinate system, as illustrated in figures 1(a) and (b), respectively. We consider a nematic material with typical refractive indices $n_\perp = 1.5$ and $n_\parallel = 1.7$, where symbols $(\perp, \parallel)$ refer to directions perpendicular and parallel to **n**, respectively. Moreover, we used splay-to-bend and twist-to-bend ratios for the Frank elastic constants $K_1/K_3 = 2/3$ and $K_2/K_3 = 1/2$ as typical values. Note that these values of the material parameters are chosen to be representative of common nematic liquid crystals (for example, see [15]). In fact, none of our conclusions is qualitatively altered when choosing the actual values of a given material.

The optical properties of these structures are calculated in the plane wave approximation, therefore all variables depend on coordinate z and time t only. The light propagation problem is solved by using the Berreman 4×4 matrix approach [16] and taking into account that, inside the nematic, the light is coupled to the Euler–Lagrange equations that govern the dynamics of the director [17]. We also introduce the reduced spatial coordinate $\xi = z/L$ and time $\tau = t/\tau_{H,P}$ where we defined the geometry-dependent characteristic times $\tau_H = \gamma_1 L^2/(\pi^2 K_3)$ [18, 19] and $\tau_P = \gamma_1 L^2/(\pi^2 K_2)$ [20], γ_1 being the rotational viscosity.

The director is represented by the usual spherical angles Θ and Φ following $\mathbf{n} = (\sin\Theta\cos\Phi, \sin\Theta\sin\Phi, \cos\Theta)$. The H and P geometries are characterized by different boundary conditions for the director at $\xi = 0$ and $\xi = 1$. In the homeotropic case, $\mathbf{n}(0,\tau) = \mathbf{n}(1,\tau) = \mathbf{e}_z$ and the director representation is

$$\mathbf{n}_H = (\sin\Theta_H\cos\Phi_H, \sin\Theta_H\sin\Phi_H, \cos\Theta_H), \quad (1)$$

with

$$\Theta_H(\xi,\tau) = \sum_{m\geqslant 1} \Theta_H^{(m)}(\tau)\sin(m\pi\xi), \quad (2)$$

$$\Phi_H(\xi,\tau) = \Phi_H^{(0)}(\tau) + \sum_{m\geqslant 1} \Phi_H^{(m)}(\tau)\frac{\sin[(m+1)\pi\xi]}{\sin(\pi\xi)}, \quad (3)$$

where m is an integer, whereas in the planar case the director lies in the plane (x, y) with $\mathbf{n}(0,\tau) = \mathbf{n}(1,\tau) = \mathbf{e}_x$, hence

$$\mathbf{n}_P = (\cos\Phi_P, \sin\Phi_P, 0), \quad (4)$$

with

$$\Phi_P(\xi,\tau) = \sum_{m\geqslant 1} \Phi_P^{(m)}(\tau)\sin(m\pi\xi). \quad (5)$$

In practice, we retain a large enough number of polar and azimuthal modes (i.e. sums that appear in equations (2), (3), (5) are truncated) in order to ensure accurate results, which is done following previous works devoted to nematic slab alone

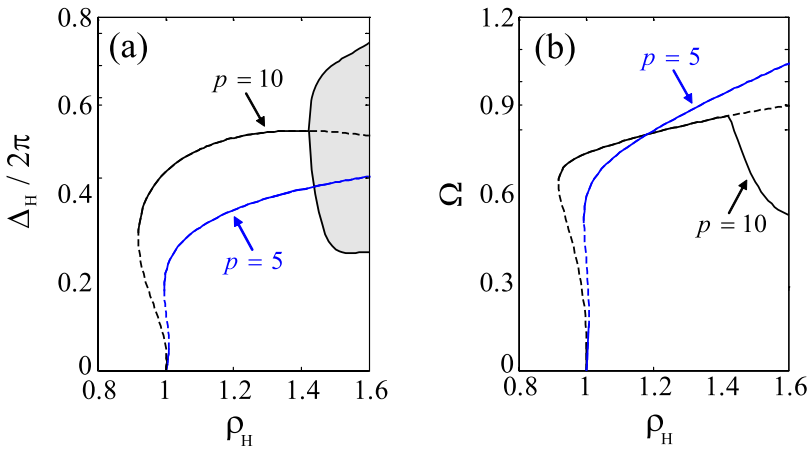

Figure 2. H slab alone. Total phase delay Δ_H (a) and director precession angular velocity $\Omega = d\Phi_H^{(0)}/d\tau$ (b) versus intensity for two different nematic thicknesses $L = p\lambda$ ($p = 5$ and 10), where $\lambda = \lambda_0/n_\perp$ is the wavelength in the unperturbed nematic. Solid (dashed) curves refer to stable (unstable) states. The gray region in (a) corresponds to the range of values explored during the quasi-periodic regime.

in the case H [18, 19] and P [20]. We introduce the (adiabatic) total phase delay Δ between the extraordinary (e) and ordinary (o) waves due to the nematic layer (which turns out to be a measure of the reorientation associated with the polar degree of freedom of the director). Again, distinction must be made between H and P cases. In the homeotropic case

$$\Delta_H(\tau) = \kappa \int_0^1 [n_{\text{eff}}(\xi, \tau) - n_\perp]\, d\xi, \tag{6}$$

with $n_{\text{eff}} = n_\parallel n_\perp/(n_\parallel^2 \cos^2\Theta_H + n_\perp^2 \sin^2\Theta_H)^{1/2}$, $\kappa = 2\pi L/\lambda_0$, and λ_0 is the incident wavelength in free space, whereas the condition $\Theta_P = \pi/2$ in the planar case imposes a constant phase delay

$$\Delta_P = \kappa(n_\parallel - n_\perp). \tag{7}$$

Finally, we define the reduced incident light intensities as $\rho_H = I_{\text{inc}}/I_H$ in the homeotropic case, where I_{inc} is the incident intensity and $I_H = 2\pi^2 c K_3 n_\parallel^2/[(n_\parallel^2 - n_\perp^2)n_\perp L^2]$ is the Fréedericksz threshold (i.e. the intensity above which the initial director state $\mathbf{n}_0$ is unstable) for circularly polarized light for a slab alone [17], whereas $\rho_P = I_{\text{inc}}/I_P$ with $I_P = 8\pi^2 c K_2 n_\parallel (n_\parallel - n_\perp)/[\lambda^2(n_\parallel + n_\perp)]$ in the planar case [20], where c is the speed of light in free space.

2.2. Light–matter interaction geometries

A general feature of the optical reordering of liquid crystals is its strong dependence on the light–matter interaction geometry, namely the director field at rest and the incidence angle, polarization, and intensity of the incident light field. Therefore a preliminary analysis is performed for the H and P cases from the knowledge of the reorientation dynamics for a nematic slab alone (i.e. without periodic structure) in order to identify situations that will potentially exhibit a dynamical optical response.

Homeotropic case. The optical reordering of a homeotropic nematic film has been intensively studied for normal or oblique incidence and for a varied set of incident beam polarization states, be it linear, elliptical, circular, or unpolarized. Various static, periodic, quasi-periodic, and aperiodic reorientation dynamics have been predicted and observed (see [8] for a review). The circular polarization case at normal incidence is a representative example for which periodic, quasi-periodic, and chaotic rotations (see [21] and references therein) have all been reported. Therefore, it seems reasonable to expect dynamical behavior too when a periodic structure is at work. However, the use of a thin nematic slab can be a crippling drawback since the light-induced dynamical richness declines as the thickness decreases. This is illustrated in figure 2 where the phase delay Δ_H, and the collective director precession angular velocity, $\Omega = d\Phi_H^{(0)}/d\tau$, are plotted as a function of the reduced intensity in figures 2(a) and (b), respectively, for two different thicknesses. It is known that these two parameters are relevant when dealing with the optically induced reorientation dynamics of nematic films [18, 19]. Indeed, the phase delay is related to the characteristic director reorientation amplitude, namely $\Delta_H \propto \Theta_H^2$ in the limit of small Θ_H, whereas the angular velocity is related to the azimuthal motion of the director. Above a light intensity threshold, the initial director orientation is unstable and $\Theta_H \neq 0$. Then, polarization changes associated with reorientation lead to light angular momentum deposition into the liquid crystal. The director is therefore put into rotation around the direction of propagation of the excitation light, $\Omega \neq 0$ [22]. Moreover, above a secondary threshold, the uniform rotation of the director can bifurcate towards a non-uniform rotation regime [18] where director precession is coupled to a nutation motion (i.e. $\Omega \neq 0$ with $\partial\Delta_H/\partial\tau \neq 0$). From figure 2, we see that such a precession-nutation regime disappears below a typical cell thickness that corresponds to $L = 2$–3 μm for typical wavelength $\lambda_0 = 600$ nm. The typical reorientation dynamics diagram observed for thick cells ($L \sim 100$ μm, see [18]) is thus qualitatively preserved in our case, where $L = 5$ μm.

Planar case. The planar alignment geometry for nematics at normal incidence has been much less studied than its homeotropic counterpart. To our knowledge, this geometry

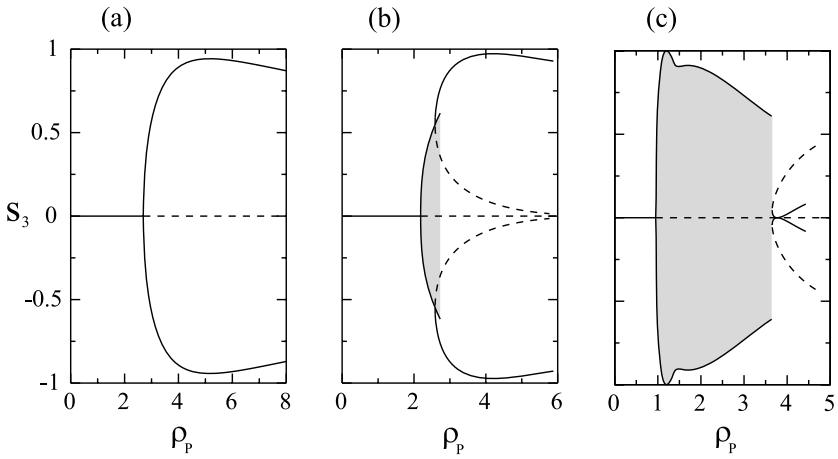

Figure 3. P slab alone. Output reduced third Stokes parameter s_3 versus intensity for three different nematic thicknesses that correspond to $\Delta_P/\pi = 0.5$ (a), 0.8 (b), and 1.6 (c). Solid (dashed) curves refer to stable (unstable) states. The gray regions in (b) and (c) correspond to the range of values explored during the oscillatory regime.

has only been considered in [23] and no further studies have been performed on it during the past two decades. This might be explained by a (twist) Fréedericksz transition threshold predicted to be up to three orders of magnitude larger than the homeotropic case, thus preventing experimental observation. Moreover, the above-threshold director distortions have been predicted to be static whatever the light intensity [23], hence limiting the need for a deeper analysis. Nevertheless, very recently, the planar geometry has attracted a renewal of interest following a seemingly experimentally accessible intensity threshold using a periodic structure [12].

In fact, the case of a planar slab alone was revisited in [20] where it is rigorously demonstrated that the reorientation threshold is significantly lower than previously predicted [23]. Moreover, a static distorted state is expected above the reorientation threshold only for optically thin enough liquid crystal layers, $\Delta_P/\pi < 0.64$ [20], whereas a dynamical regime that takes place via a Hopf bifurcation is predicted otherwise, which has been missed so far [23]. A secondary instability (heteroclinic bifurcation), which eventually leads to a static regime, has also been predicted to be associated ($0.64 < \Delta_P/\pi < 1$), or not ($\Delta_P/\pi > 1$), with hysteresis behavior [20]. In order to summarize these results it is useful to introduce the reduced third Stokes component [24], s_3, at the output of the nematic film. Indeed $s_3 = 0$ in the absence of reorientation since the linear incident polarization state is unaltered in that case, whereas $s_3 \neq 0$ as soon as $\Phi_P \neq 0$. Moreover, a time-dependent director reorientation can be retrieved from output polarization dynamics, hence $ds_3/d\tau \neq 0$. Typical scenarios when the reduced intensity is taken as the control parameter are summarized in figure 3 for three representative optical thicknesses that correspond to $\Delta_P/\pi = 0.5$ (a), 0.8 (b), and 1.6 (c).

Since $L = 5\ \mu$m corresponds to $\Delta_P/\pi \sim 4$ in the visible range with the present choice of material parameters, a non-trivial sequence of nonlinear reorientation dynamics is *a priori* expected. Importantly, note that the chosen film thickness is nevertheless thin enough to prevent the influence of stimulated scattering, in contrast to thick cells where full polarization conversion can be observed [25, 26]. Indeed, the latter phenomenon is all the more important as the ratio $\Lambda = L(n_\parallel - n_\perp)/\lambda_0$ between the thickness and the intensity modulation grating period arising from the coherent superposition of extraordinary and ordinary waves is large compared to unity. Since $\Lambda \sim 2$ in our case, the stimulated scattering can therefore be neglected in our approach.

Finally, we further consider the case H under circularly polarized excitation at normal incidence and the case P under ordinary linearly polarized excitation at normal incidence, as sketched in figures 1(a) and (b), respectively.

3. Spectrally modulated optomechanical efficiency

In both H and P cases, the incident beam polarization corresponds to an ordinary wave for the nematic at rest and the optical torque density exerted on $\mathbf{n}_0$ is thus zero. However, the orientational state $\mathbf{n} = \mathbf{n}_0$ is linearly unstable with respect to fluctuations when the light intensity is high enough to overcome the restoring elastic torque density that originates from the cell walls, which defines the optical Fréedericksz transition threshold [17]. The presence of the periodic structure does not suppress the optical destabilization scenario, but enriches it. Indeed, the reduced thresholds $\rho_{H,th}$ (figure 4(a)) and $\rho_{P,th}$ (figure 4(b)) strongly depend on the excitation beam wavelength λ_0 inside the bandgap, as already discussed in detail in the homeotropic case [11, 13]. Namely, the defect modes evidenced by sharp peaks in the transmission spectrum T_H (figure 4(c)) are associated to an enhanced light confinement in the nematic defect layer that leads to a significant reduction (up to several orders of magnitude) of the required incident intensity to trigger the liquid crystal reorientation (figure 4(a)).

In the planar case, a strongly modulated reorientation threshold is observed too, as shown in (figure 4(b)), however, its fine structure is more complex than its homeotropic counterpart. Indeed the spectrum of $\rho_{P,th}$ exhibits two

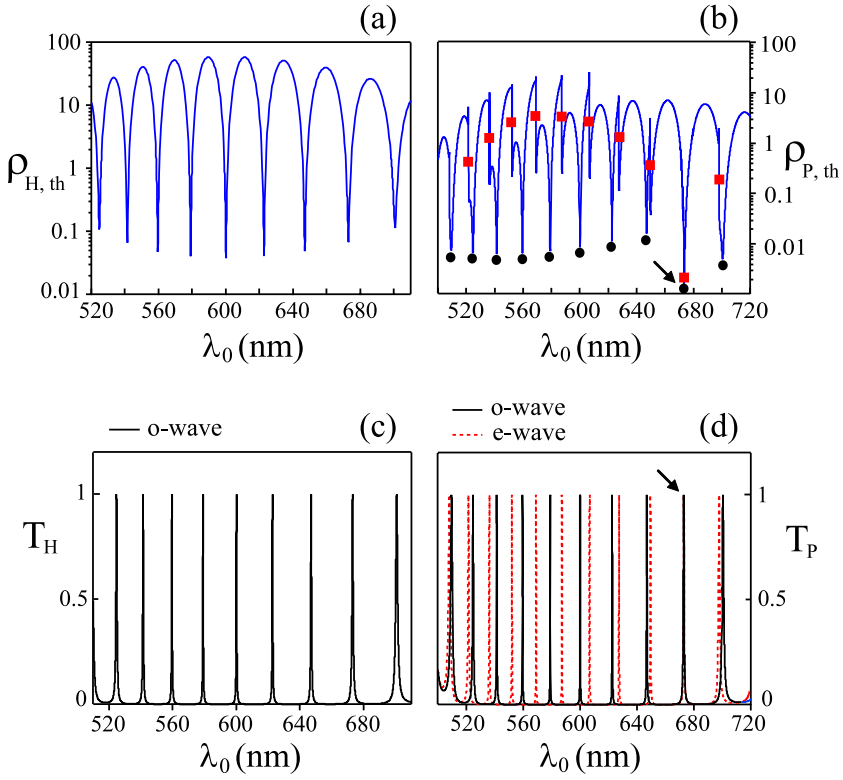

Figure 4. Reduced thresholds $\rho_{H,th}$ (a) and $\rho_{P,th}$ (b) and transmission spectra T_H (c) and T_P (d) at rest ($\mathbf{n} = \mathbf{n}_0$). In (b), circle (square) symbols refer to the ordinary (extraordinary) mode shown in (d).

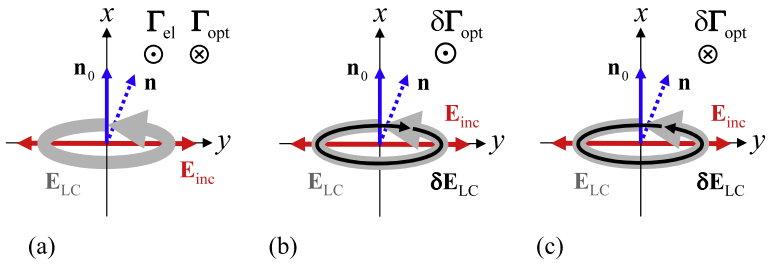

Figure 5. Qualitative interpretation of the asymmetric resonance lineshape nearby an extraordinary defect mode in the planar geometry. Elastic and optical torque densities exerted on the director in the presence of an orientational fluctuation are shown in (a) for a slab alone whereas (b) and (c) illustrate the negative and positive feedback from the periodic structure for $\lambda_0 \lesssim \lambda_d^e$ and $\lambda_0 \gtrsim \lambda_d^e$, respectively.

sets of resonances with either symmetric (circle symbols in figure 4(b)) or asymmetric (square symbols in figure 4(b)) lineshape that are related to the o- and e-defect mode wavelengths λ_d^o and λ_d^e, respectively. Such a behavior is a direct manifestation of the competing influence of the o- and e-modes. On the one hand, symmetric resonance lineshapes in the planar case are reminiscent of the incident ordinary polarized light field enhancement in the nematic defect layer when $\lambda_0 \approx \lambda_d^o$, as in the homeotropic case. On the other hand, the origin of the asymmetric resonance lineshapes when $\lambda_0 \approx \lambda_d^e$ can be qualitatively grasped by considering a fluctuation around the initial state $\mathbf{n}_0$ for a planar slab alone, see figure 5(a). The elastic torque density ($\mathbf{\Gamma}_{el}$) driven by the cell walls tends to restore the director perturbation whereas the subsequent polarization changes (see typical polarization state inside the liquid crystal labeled as $\mathbf{E}_{LC}$ in figure 5) are associated to a spin angular momentum deposition [22], hence an optical torque density ($\mathbf{\Gamma}_{opt}$), that tends to increase the initial amplitude of the fluctuation, as illustrated in figure 5(a). The influence of the periodic structure is addressed by noting that (i) the phase of the o-wave is almost constant in the vicinity of an e-defect mode (except when $\lambda_d^o \approx \lambda_d^e$) and (ii) a π phase shift is experienced by the e-wave when the incident beam wavelength explores the resonance linewidth. Therefore, the sign of the optical feedback ($\delta\mathbf{\Gamma}_{opt}$) is either negative or positive depending on the resonance side, as shown in figures 5(b) and (c). We note here the analogy with the Fano resonance arising from the interference of resonant and non-resonant scattering waves, which is characterized by an asymmetric lineshape [27]. Indeed, a resonantly excited e-wave leads to constructive and destructive interference with an o-wave in the vicinity of an e-defect mode. When $\lambda_d^o \approx \lambda_d^e$ (i.e. $\lambda_0 \approx 673$ nm,

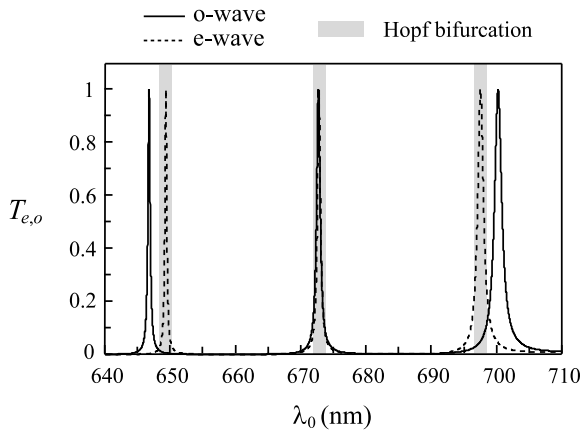

Figure 6. Spectrally modulated nature of the reorientation transition that corresponds to a stationary bifurcation except in the vicinity of e-defect modes, which is identified by gray regions, where a Hopf bifurcation takes place.

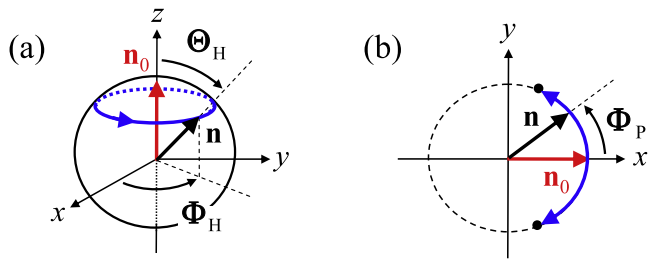

Figure 7. Director regimes in the H (a) and P (b) geometries. Uniform precession of the director around the z axis is found in the case H whereas either static distorted states (see markers) or director oscillation in the (x, y) plane are predicted in the case P.

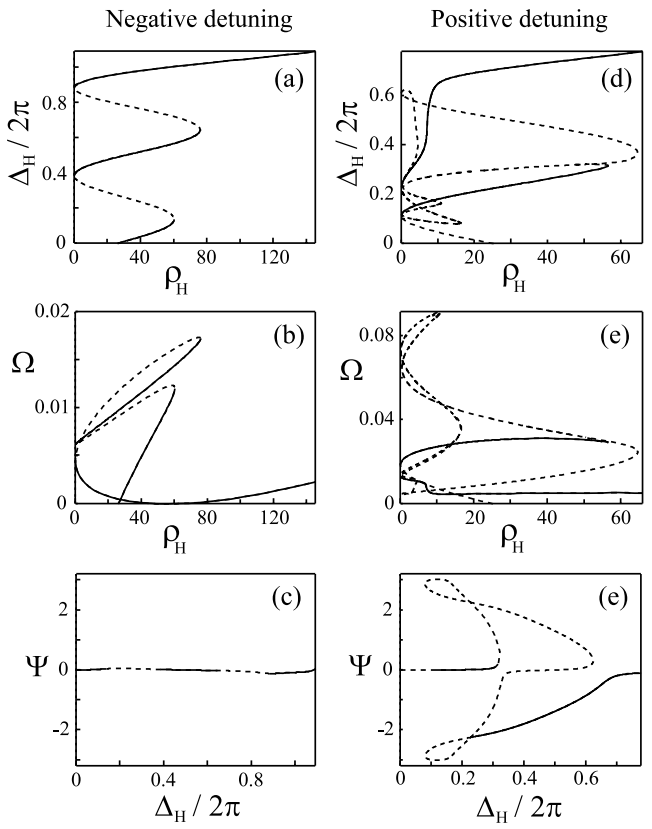

Figure 8. Director reorientation characteristics for negative (panels (a)–(c)) and positive (panels (d)–(f)) detuning $\lambda_0 - \lambda_d^o = \pm 5$ nm near the defect mode $\lambda_d^o \approx 600$ nm. The total phase delay $\Delta_H/2\pi$ and angular rotation frequency Ω versus input intensity are shown in (a), (d) and (b), (e), respectively. The total twist defined by $\Psi = \Phi_H(1, \tau) - \Phi_H(0, \tau)$ versus $\Delta_H/2\pi$ is shown in (c), (f). Solid (dashed) curves correspond to stable (unstable) regimes.

see arrow in figure 4(d)), the dephasing associated with the defect modes between the o- and e-waves is even smaller than λ_d^o and is close to λ_d^e, which eventually leads to a symmetric resonance lineshape for $\rho_{P,th}$ (see arrow in figure 4(b)).

The nature of the optical reordering transition also depends on the excitation beam wavelength. In the homeotropic case, the order of the orientational instability can be either first-or second-order depending on the detuning $\lambda_0 - \lambda_d^o$ between the pump wavelength and the nearest defect mode λ_d^o, as previously discussed for an identical structure with linearly polarized excitation [11, 13], which is a general result for homeotropic films inside a resonator under linearly polarized light [28, 29]. Indeed, the transition is first-order for positive detuning whereas it is second-order for negative detuning (see later figures 8(a) and (b) in section 4). Such behavior is therefore independent of the presence or not of an intrinsic optical bistability (i.e. for the nematic slab alone) since linearly and circularly polarized excitations are related to second- and first-order transitions, respectively. In the planar case, we also find that the order of the transition is controlled by the detuning with respect to the nearest o-defect mode, whatever the detuning between the o- and e-defect modes, but with some exception in the vicinity of the e-defect modes where a supercritical Hopf bifurcation is found (i.e. second-order transition), as illustrated in figure 6. This emphasizes the prominent role played by the e-defect modes in the case P although incident light is ordinary polarized.

4. All-optical dynamical optical response

As expected from the analysis of H and P nematic slab alone in section 2.2, we find dynamical regimes for the director reorientation above $\rho_{H,th}$ and $\rho_{P,th}$, respectively. In the case H, however, there is no nutation regime ($\partial\Theta_H/\partial\tau \neq 0$) whatever the wavelength, although uniform precession ($\partial\Phi_H/\partial\tau =$ constant) is always present. In the case P, the distorted state is static or corresponds to an oscillatory motion in the (x, y) plane. These regimes are sketched in figure 7 and next we discuss the optical response of the structure when dynamics takes place.

Homeotropic case. The uniform director nutation-free precession dynamics corresponds to a constant polar spatial profile (Θ_H) for which Δ_H is an estimate of the overall amplitude (see equation (6)). The azimuthal spatial profile is also constant but in a frame that rotates at constant angular velocity $\Omega = \partial\Phi_H/\partial\tau = d\Phi_H^{(0)}/d\tau$ around the z axis. Also, we define the overall twisted character of the distortion profile in the rotating frame as the twist angle between the output and input facets of the nematic defect layer, $\Psi = \Phi_H(1, \tau) -$

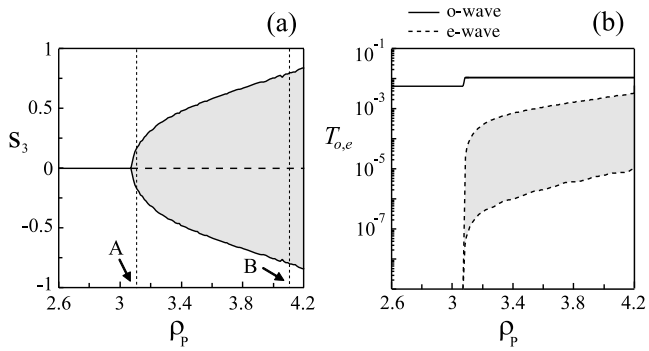

Figure 9. (a) Reduced Stokes' parameter s_3 versus input intensity where solid (dashed) curves refer to stable (unstable) states. (b) Ordinary and extraordinary transmissions T_o (solid curve) and T_e (dashed curve) versus input intensity at $\lambda_0 = 650$ nm. Gray areas correspond to the range of values explored during the dynamics.

$\Phi_H(0, \tau)$. The incident intensity dependences of these three representative quantities, Δ_H, Ω, and Ψ are shown in figure 7 for negative and positive detuning, $\lambda_0 - \lambda_d^o = \pm 5$ nm, near the defect mode $\lambda_d^o \approx 600$ nm (see figure 4(c)).

In fact, Δ_H and Ω are related to distinct features of the polarization state at the output of the structure, namely the ellipticity and the rotation rate of the polarization ellipse, whose azimuth is given by $\Phi_H(1, \tau)$ [18, 22] (rigorously, non-adiabatic light propagation when $\Psi \neq 0$ slightly modifies this correspondence). Since Δ_H is time-independent, the total transmission T_H is constant and the dynamical optical response of the structure is merely contained in the polarization azimuth whatever the sign of the detuning. The intensity dependence of the optical response, however, strongly depends on wavelength, as shown in figure 8. Indeed, for negative detuning, the overall reorientation picture is very similar to the case of linearly polarized excitation [11], as shown in figure 8(a). This is due to the almost untwisted distortion profile, $\Phi_H^{(m)} \ll 1$, hence $\Psi \ll 1$, see figure 8(c). This contrasts with the case of positive detuning where a complex reorientation diagram is found (figure 8(c)) as a result of large twist amplitude and associated significant non-adiabatic light propagation effects. Such a behavior is not observed for a homeotropic slab alone and is the signature of the interaction between o- and e-defect modes that are no longer degenerate when $\mathbf{n} \neq \mathbf{n}_0$.

Planar case. Static or oscillatory regimes are found depending on the incident wavelength and intensity. Static distortions are found for almost any wavelength except in the vicinity of extraordinary defect modes where oscillatory dynamics appears via a Hopf bifurcation, as illustrated in figure 9(a). In that case, the output optical response exhibits time-dependent o- and e-transmissions, as shown in figure 9(b); however, note that the modulation depths of $T_o(\tau)$ are much less pronounced than that of $T_e(\tau)$ and $T_e \ll T_o$. Details of the dynamics are illustrated in figure 10 near and well above the threshold at intensities that correspond to labels A and B in figure 9(a), respectively. As expected from a Hopf bifurcation, a single frequency characterizes the dynamics near $\rho_{P,th}$, see figure 10(a), whereas a second frequency grows up as the intensity increases, which leads to a quasi-periodic oscillation with the subsequent appearance of harmonic frequencies and frequency mixing that are clearly seen in the Fourier spectrum of the time-dependent transmission, see figure 10(b). The corresponding spatio-temporal director dynamics, $\Phi_P(\xi, \tau)$, is shown in figures 10(c) and (d). Aperiodic dynamics, which has not been predicted for a planar slab alone [20], is also found in simulations at higher intensities (not shown here),

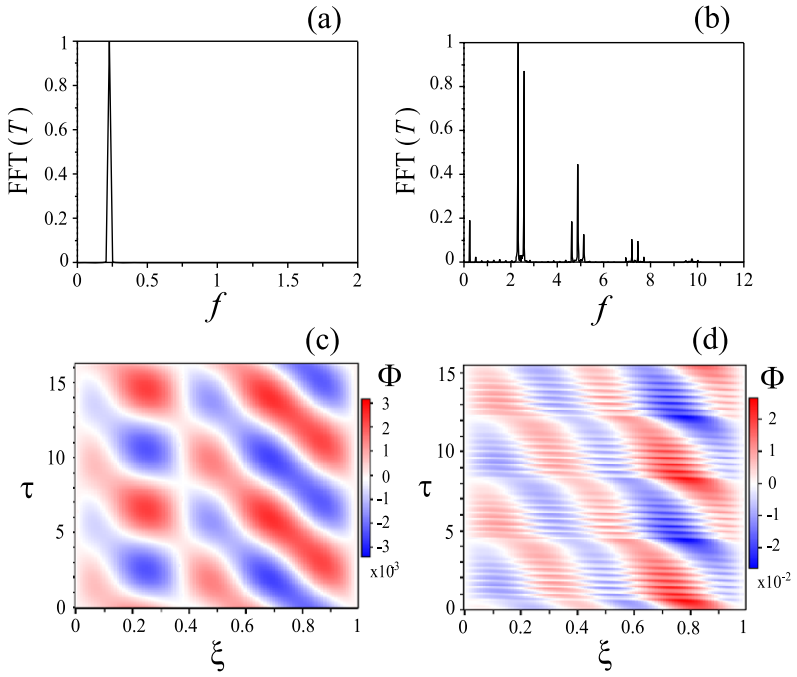

Figure 10. Fourier spectra of the time-dependent total transmission ((a) and (b)) and spatio-temporal dynamics of the azimuthal spatial profile $\Phi_P(\xi, \tau)$ ((c) and (d)) just above the Hopf bifurcation threshold (see A in figure 9(a)) and far above the threshold (see B in figure 9(a)).

which emphasizes how the presence of the periodic structure compares with the homeotropic case.

5. Conclusion

The dynamical response of all-optical liquid crystal infiltrated photonic structures has been discussed in two light–matter interaction geometries that correspond to a circularly (linearly) polarized incident beam impinging at normal incidence onto a one-dimensional periodic structure in which is embedded a nematic liquid crystal defect layer with homeotropic (planar) alignment (i.e. perpendicular (parallel) to the layer). In both cases the incident beam polarization state corresponds to an ordinary wave and optical reordering takes place only above a threshold for the input intensity that is much smaller than the usual optical Fréedericksz transition threshold reduced with respect to in the vicinity of ordinary defect modes. It has been shown that self-sustained dynamics of the output light polarization and/or intensity can take place in contrast with all previous attempts discussed so far, thus paving the way towards an all-optical dynamical response of photonic structures using liquid crystals. For example, this could be used to exploit dynamically the recently introduced concept of reversible optical nonreciprocity [30].

Acknowledgments

This work was supported by the Australian Research Council through the Discovery Project and Centre of Excellence programs and by the France–Australia cooperation project 21337 of CNRS.

References

[1] Yablonovitch E 1987 *Phys. Rev. Lett.* **58** 2059
[2] John S 1987 *Phys. Rev. Lett.* **58** 2486
[3] Joannopoulos J, Meade R and Winn J N 1995 *Photonic Crystals: Molding the Flow of Light* (Princeton, NY: Princeton University Press)
[4] Juodkazis S, Mizeikis V, Matsuo S, Ueno K and Misawa H 2008 *Bull. Chem. Soc. Japan* **4** 411
[5] Soljacic M and Joannopoulos J D 2004 *Nat. Mater.* **3** 211
[6] Busch K and John S 1999 *Phys. Rev. Lett.* **83** 967
[7] Yoshino K, Shimoda Y, Kawagishi Y, Nakayama K and Ozaki M 1999 *Appl. Phys. Lett.* **75** 932
[8] Demeter G and Krimer D O 2007 *Phys. Rep.* **448** 133
[9] Khoo I C 2009 *Phys. Rep.* **471** 221
[10] Miroshnichenko A E, Pinkevych I and Kivshar Y S 2006 *Opt. Express* **14** 2839
[11] Miroshnichenko A E, Brasselet E and Kivshar Y S 2008 *Appl. Phys. Lett.* **92** 253306
[12] Laudyn U A, Miroshnichenko A E, Krolikowski W, Chen D F, Kivshar Y S and Karpierz M A 2008 *Appl. Phys. Lett.* **92** 203304
[13] Miroshnichenko A E, Brasselet E and Kivshar Y S 2008 *Phys. Rev.* A **78** 053823
[14] Brasselet E, Miroshnichenko A E, Chen D F, Krolikowski W and Kivshar Y S 2009 *Opt. Lett.* **34** 488
[15] de Gennes P G 1974 *The Physics of Liquid Crystals* (Oxford: Oxford University Press)
[16] Berreman D W 1972 *J. Opt. Soc. Am.* **62** 502
[17] Tabiryan N V, Sukhov A V and Zel'dovich B Y 1986 *Mol. Cryst. Liquid Cryst.* **136** 1
[18] Brasselet E, Galstian T V, Dubé L J, Krimer D O and Kramer L 2005 *J. Opt. Soc. Am.* B **22** 1671
[19] Krimer D O, Kramer L, Brasselet E, Galstian T V and Dubé L J 2005 *J. Opt. Soc. Am.* B **22** 1681
[20] Krimer D O 2009 *Phys. Rev.* E **79** 030702(R)
[21] Brasselet E, Piccirillo B and Santamato E 2008 *Phys. Rev.* E **78** 031703
[22] Santamato E, Daino B, Romagnoli M, Settembre M and Shen Y R 1986 *Phys. Rev. Lett.* **57** 2423
[23] Santamato E, Abbate G, Maddalena P and Shen Y R 1987 *Phys. Rev.* A **36** 2389
[24] Born M and Wolf E 1999 *Principles of Optics* 7th edn (Cambridge: Cambridge University Press)
[25] Khoo I C and Ding J 2002 *Appl. Phys. Lett.* **81** 2496
[26] Khoo I C and Diaz A 2003 *Phys. Rev.* E **68** 042701
[27] Miroshnichenko A E, Flach S and Kivshar Y S 2010 *Rev. Mod. Phys.* at press
[28] Marquis F and Meystre P 1987 *Opt. Commun.* **62** 409
[29] D'Alessandro G and Wheeler A A 2003 *Phys. Rev.* A **67** 023816
[30] Miroshnichenko A E, Brasselet E and Kivshar Y S 2010 *Appl. Phys. Lett.* **96** 063302